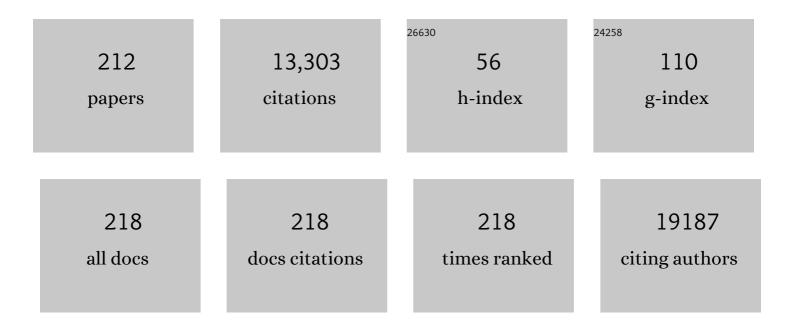
Zonghoon Lee

List of Publications by Year in descending order

Source: https://exaly.com/author-pdf/8734803/publications.pdf Version: 2024-02-01



#	Article	IF	CITATIONS
1	Determination of the Local Chemical Structure of Graphene Oxide and Reduced Graphene Oxide. Advanced Materials, 2010, 22, 4467-4472.	21.0	1,044
2	Substrate-Free Gas-Phase Synthesis of Graphene Sheets. Nano Letters, 2008, 8, 2012-2016.	9.1	691
3	Grain Boundary Mapping in Polycrystalline Graphene. ACS Nano, 2011, 5, 2142-2146.	14.6	566
4	Multicomponent electrocatalyst with ultralow Pt loading and high hydrogen evolution activity. Nature Energy, 2018, 3, 773-782.	39.5	542
5	Fluorographene: A Wide Bandgap Semiconductor with Ultraviolet Luminescence. ACS Nano, 2011, 5, 1042-1046.	14.6	394
6	Growth of High-Crystalline, Single-Layer Hexagonal Boron Nitride on Recyclable Platinum Foil. Nano Letters, 2013, 13, 1834-1839.	9.1	336
7	Al–Mg alloy engineered with bimodal grain size for high strength and increased ductility. Scripta Materialia, 2003, 49, 297-302.	5.2	330
8	Ordered mesoporous porphyrinic carbons with very high electrocatalytic activity for the oxygen reduction reaction. Scientific Reports, 2013, 3, 2715.	3.3	282
9	Direct exfoliation and dispersion of two-dimensional materials in pure water via temperature control. Nature Communications, 2015, 6, 8294.	12.8	277
10	Multiply folded graphene. Physical Review B, 2011, 83, .	3.2	269
11	Deformation behavior of bimodal nanostructured 5083 Al alloys. Metallurgical and Materials Transactions A: Physical Metallurgy and Materials Science, 2005, 36, 957-965.	2.2	227
12	Highâ€Performance Hydrogen Evolution by Ru Single Atoms and Nitridedâ€Ru Nanoparticles Implanted on Nâ€Đoped Graphitic Sheet. Advanced Energy Materials, 2019, 9, 1900931.	19.5	224
13	Metallic NEMS components fabricated from nanocomposite Al–Mo films. Nanotechnology, 2006, 17, 3063-3070.	2.6	223
14	Single-crystal, large-area, fold-free monolayer graphene. Nature, 2021, 596, 519-524.	27.8	205
15	Fast Synthesis of High-Performance Graphene Films by Hydrogen-Free Rapid Thermal Chemical Vapor Deposition. ACS Nano, 2014, 8, 950-956.	14.6	195
16	A tri-modal aluminum based composite with super-high strength. Scripta Materialia, 2005, 53, 481-486.	5.2	191
17	Controllable synthesis of molybdenum tungsten disulfide alloy for vertically composition-controlled multilayer. Nature Communications, 2015, 6, 7817.	12.8	188
18	Microstructural study on degradation mechanism of layered LiNi0.6Co0.2Mn0.2O2 cathode materials by analytical transmission electron microscopy. Journal of Power Sources, 2016, 307, 641-648.	7.8	187

#	Article	IF	CITATIONS
19	Chemically induced transformation of chemical vapour deposition grown bilayer graphene into fluorinated single-layer diamond. Nature Nanotechnology, 2020, 15, 59-66.	31.5	184
20	Lowâ€Temperature Synthesis of Largeâ€6cale Molybdenum Disulfide Thin Films Directly on a Plastic Substrate Using Plasmaâ€Enhanced Chemical Vapor Deposition. Advanced Materials, 2015, 27, 5223-5229.	21.0	180
21	Ultralow-dielectric-constant amorphous boron nitride. Nature, 2020, 582, 511-514.	27.8	173
22	Carbon Nanotubes/Heteroatomâ€Doped Carbon Core–Sheath Nanostructures as Highly Active, Metalâ€Free Oxygen Reduction Electrocatalysts for Alkaline Fuel Cells. Angewandte Chemie - International Edition, 2014, 53, 4102-4106.	13.8	168
23	Anomalous polarization dependence of Raman scattering and crystallographic orientation of black phosphorus. Nanoscale, 2015, 7, 18708-18715.	5.6	167
24	Synthesis of wafer-scale uniform molybdenum disulfide films with control over the layer number using a gas phase sulfur precursor. Nanoscale, 2014, 6, 2821.	5.6	166
25	The Origin of Improved Electrical Double‣ayer Capacitance by Inclusion of Topological Defects and Dopants in Graphene for Supercapacitors. Angewandte Chemie - International Edition, 2016, 55, 13822-13827.	13.8	161
26	Low-temperature synthesis of 2D MoS ₂ on a plastic substrate for a flexible gas sensor. Nanoscale, 2018, 10, 9338-9345.	5.6	142
27	Large-area single-crystal AB-bilayer and ABA-trilayer graphene grown on a Cu/Ni(111) foil. Nature Nanotechnology, 2020, 15, 289-295.	31.5	141
28	Mechanical properties of an ultrafine-grained Al-7.5 Pct Mg alloy. Metallurgical and Materials Transactions A: Physical Metallurgy and Materials Science, 2003, 34, 603-613.	2.2	139
29	Highly Oriented Monolayer Graphene Grown on a Cu/Ni(111) Alloy Foil. ACS Nano, 2018, 12, 6117-6127.	14.6	132
30	Direct Imaging of Softâ ``Hard Interfaces Enabled by Graphene. Nano Letters, 2009, 9, 3365-3369.	9.1	127
31	Atomic Scale Study on Growth and Heteroepitaxy of ZnO Monolayer on Graphene. Nano Letters, 2017, 17, 120-127.	9.1	120
32	Microstructure and microhardness of cryomilled bulk nanocrystalline Al?7.5%Mg alloy consolidated by high pressure torsion. Scripta Materialia, 2004, 51, 209-214.	5.2	106
33	Hydrophobicity of Rare Earth Oxides Grown by Atomic Layer Deposition. Chemistry of Materials, 2015, 27, 148-156.	6.7	106
34	2D Transition Metal Dichalcogenide Heterostructures for p―and nâ€Type Photovoltaic Selfâ€Powered Gas Sensor. Advanced Functional Materials, 2020, 30, 2003360.	14.9	102
35	Immiscible bi-metal single-atoms driven synthesis of electrocatalysts having superb mass-activity and durability. Applied Catalysis B: Environmental, 2020, 270, 118896.	20.2	102
36	Tensile Deformation and Fracture Mechanism of Bulk Bimodal Ultrafine-Grained Al-Mg Alloy. Metallurgical and Materials Transactions A: Physical Metallurgy and Materials Science, 2010, 41, 795-801.	2.2	98

#	Article	IF	CITATIONS
37	High-resolution electrohydrodynamic inkjet printing of stretchable metal oxide semiconductor transistors with high performance. Nanoscale, 2016, 8, 17113-17121.	5.6	97
38	Creating Pores on Graphene Platelets by Lowâ€Temperature KOH Activation for Enhanced Electrochemical Performance. Small, 2016, 12, 2376-2384.	10.0	95
39	High-Performance Gas Sensor Using a Large-Area WS _{2<i>x</i>} Se _{2–2<i>x</i>} Alloy for Low-Power Operation Wearable Applications. ACS Applied Materials & Interfaces, 2018, 10, 34163-34171.	8.0	93
40	Raman Signatures of Polytypism in Molybdenum Disulfide. ACS Nano, 2016, 10, 1948-1953.	14.6	92
41	Controlled Folding of Single Crystal Graphene. Nano Letters, 2017, 17, 1467-1473.	9.1	92
42	Route to the Smallest Doped Semiconductor: Mn ²⁺ -Doped (CdSe) ₁₃ Clusters. Journal of the American Chemical Society, 2015, 137, 12776-12779.	13.7	91
43	Wafer-scale production of patterned transition metal ditelluride layers for two-dimensional metal–semiconductor contacts at the Schottky–Mott limit. Nature Electronics, 2020, 3, 207-215.	26.0	91
44	Bimodal microstructure and deformation of cryomilled bulk nanocrystalline Al–7.5Mg alloy. Materials Science & Engineering A: Structural Materials: Properties, Microstructure and Processing, 2005, 410-411, 462-467.	5.6	87
45	Structural and Optical Properties of Single- and Few-Layer Magnetic Semiconductor CrPS ₄ . ACS Nano, 2017, 11, 10935-10944.	14.6	85
46	Graphitization of graphene oxide films under pressure. Carbon, 2018, 132, 294-303.	10.3	84
47	Clean and highly ordered graphene synthesized in the gas phase. Chemical Communications, 2009, , 6095.	4.1	82
48	Synthesis of aligned symmetrical multifaceted monolayer hexagonal boron nitride single crystals on resolidified copper. Nanoscale, 2016, 8, 2434-2444.	5.6	81
49	A Comparison of the Corrosion Behavior of Nanocrystalline and Conventional Al 5083 Samples. Corrosion, 2006, 62, 152-161.	1.1	77
50	Self-Limiting Layer Synthesis of Transition Metal Dichalcogenides. Scientific Reports, 2016, 6, 18754.	3.3	74
51	Interface-Controlled Synthesis of Heterodimeric Silver–Carbon Nanoparticles Derived from Polysaccharides. ACS Nano, 2014, 8, 11377-11385.	14.6	67
52	Superaerophobic graphene nano-hills for direct hydrazine fuel cells. NPG Asia Materials, 2017, 9, e378-e378.	7.9	64
53	Atomic-scale dynamics of triangular hole growth in monolayer hexagonal boron nitride under electron irradiation. Nanoscale, 2015, 7, 10600-10605.	5.6	63
54	Role of Graphene in Water-Assisted Oxidation of Copper in Relation to Dry Transfer of Graphene. Chemistry of Materials, 2017, 29, 4546-4556.	6.7	63

#	Article	IF	CITATIONS
55	Oxidation behavior of graphene-coated copper at intrinsic graphene defects of different origins. Nature Communications, 2017, 8, 1549.	12.8	60
56	Monodisperse Al3(LiScZr) core/shell precipitates in Al alloys. Scripta Materialia, 2008, 58, 529-532.	5.2	57
57	Remarkably enhanced catalytic activity by the synergistic effect of palladium single atoms and palladium–cobalt phosphide nanoparticles. Nano Energy, 2020, 78, 105166.	16.0	57
58	Interface rich CuO/Al ₂ CuO ₄ surface for selective ethylene production from electrochemical CO ₂ conversion. Energy and Environmental Science, 2022, 15, 2397-2409.	30.8	54
59	Hydrogen-Enriched Reduced Graphene Oxide with Enhanced Electrochemical Performance in Lithium Ion Batteries. Chemistry of Materials, 2015, 27, 266-275.	6.7	53
60	Catalytic Conversion of Hexagonal Boron Nitride to Graphene for In-Plane Heterostructures. Nano Letters, 2015, 15, 4769-4775.	9.1	52
61	Sulfur-Modified Graphitic Carbon Nitride Nanostructures as an Efficient Electrocatalyst for Water Oxidation. Small, 2017, 13, 1603893.	10.0	52
62	Chemical Vapor-Deposited Hexagonal Boron Nitride as a Scalable Template for High-Performance Organic Field-Effect Transistors. Chemistry of Materials, 2017, 29, 2341-2347.	6.7	52
63	Atomicâ€Level Customization of 4 in. Transition Metal Dichalcogenide Multilayer Alloys for Industrial Applications. Advanced Materials, 2019, 31, e1901405.	21.0	52
64	Conversionless efficient and broadband laser light diffusers for high brightness illumination applications. Nature Communications, 2020, 11, 1437.	12.8	52
65	On-stack two-dimensional conversion of MoS ₂ into MoO ₃ . 2D Materials, 2017, 4, 014003.	4.4	51
66	Porous Two-Dimensional Monolayer Metal–Organic Framework Material and Its Use for the Size-Selective Separation of Nanoparticles. ACS Applied Materials & Interfaces, 2017, 9, 28107-28116.	8.0	51
67	Crystal Structure Evolution of Individual Graphene Islands During CVD Growth on Copper Foil. Advanced Materials, 2013, 25, 6744-6751.	21.0	50
68	Dynamics of Triangular Hole Growth in Monolayer Hexagonal Boron Nitride under Electron Irradiation. Microscopy and Microanalysis, 2015, 21, 739-740.	0.4	49
69	Ultrastiff, Strong, and Highly Thermally Conductive Crystalline Graphitic Films with Mixed Stacking Order. Advanced Materials, 2019, 31, e1903039.	21.0	49
70	Large-area niobium disulfide thin films as transparent electrodes for devices based on two-dimensional materials. Nanoscale, 2018, 10, 1056-1062.	5.6	44
71	Nucleation and Growth of the HfO ₂ Dielectric Layer for Graphene-Based Devices. Chemistry of Materials, 2015, 27, 5868-5877.	6.7	43
72	Catalytic chemical vapor deposition of large-area uniform two-dimensional molybdenum disulfide using sodium chloride. Nanotechnology, 2017, 28, 465103.	2.6	42

#	Article	IF	CITATIONS
73	Microstructural evolution and deformation of cryomilled nanocrystalline Al-Ti-Cu Alloy. Metallurgical and Materials Transactions A: Physical Metallurgy and Materials Science, 2003, 34, 1473-1481.	2.2	40
74	Effect of Al ₂ O ₃ Deposition on Performance of Top-Gated Monolayer MoS ₂ -Based Field Effect Transistor. ACS Applied Materials & Interfaces, 2016, 8, 28130-28135.	8.0	40
75	Uniform, large-area self-limiting layer synthesis of tungsten diselenide. 2D Materials, 2016, 3, 014004.	4.4	40
76	Size-dependent interaction of Au nanoparticles and graphene sheet. Chemical Communications, 2011, 47, 3610.	4.1	39
77	Rupturing C60Molecules into Graphene-Oxide-like Quantum Dots: Structure, Photoluminescence, and Catalytic Application. Small, 2015, 11, 5296-5304.	10.0	39
78	Wafer-scale monolayer MoS ₂ grown by chemical vapor deposition using a reaction of MoO ₃ and H ₂ S. Journal of Physics Condensed Matter, 2016, 28, 184002.	1.8	39
79	Simultaneous improvement in electrical and thermal properties of interface-engineered BiSbTe nanostructured thermoelectric materials. Journal of Alloys and Compounds, 2016, 689, 899-907.	5.5	39
80	Complete determination of the crystallographic orientation of ReX ₂ (X = S, Se) by polarized Raman spectroscopy. Nanoscale Horizons, 2020, 5, 308-315.	8.0	37
81	One-dimensional hexagonal boron nitride conducting channel. Science Advances, 2020, 6, eaay4958.	10.3	37
82	Degradation behaviors and mechanisms of MoS2 crystals relevant to bioabsorbable electronics. NPG Asia Materials, 2018, 10, 810-820.	7.9	36
83	Determination of the thickness and orientation of few-layer tungsten ditelluride using polarized Raman spectroscopy. 2D Materials, 2016, 3, 034004.	4.4	35
84	Hole Defects on Two-Dimensional Materials Formed by Electron Beam Irradiation: Toward Nanopore Devices. Applied Microscopy, 2015, 45, 107-114.	1.4	34
85	Cryomilling for the fabrication of a particulate B4C reinforced Al nanocomposite: Part II. Mechanisms for microstructural evolution. Metallurgical and Materials Transactions A: Physical Metallurgy and Materials Science, 2006, 37, 3111-3117.	2.2	33
86	Monolithic graphene oxide sheets with controllable composition. Nature Communications, 2014, 5, 3383.	12.8	31
87	Graphene Edges and Beyond: Temperature-Driven Structures and Electromagnetic Properties. ACS Nano, 2015, 9, 4669-4674.	14.6	31
88	Evidence of Local Commensurate State with Lattice Match of Graphene on Hexagonal Boron Nitride. ACS Nano, 2017, 11, 7084-7090.	14.6	31
89	Chemical mapping of a block copolymer electrolyte by low-loss EFTEM spectrum-imaging and principal component analysis. Ultramicroscopy, 2011, 111, 239-244.	1.9	30
90	Engineering Electronic Properties of Graphene by Coupling with Si-Rich, Two-Dimensional Islands. ACS Nano, 2013, 7, 301-307.	14.6	30

#	Article	IF	CITATIONS
91	runing of magnetic and transport properties in Bi <mmi:math xmlns:mml="http://www.w3.org/1998/Math/MathML" display="inline"><mmi:msub><mmi:mrow /><mmi:mn>2</mmi:mn></mmi:mrow </mmi:msub>Te<mmi:math xmlns:mml="http://www.w3.org/1998/Math/MathML" display="inline"><mmi:msub><mmi:mrow< td=""><td>3.2</td><td>30</td></mmi:mrow<></mmi:msub></mmi:math </mmi:math 	3.2	30
92	Quantum-dot light-emitting diodes utilizing CdSeâ^•ZnS nanocrystals embedded in TiO2 thin film. Applied Physics Letters, 2008, 93, .	3.3	27
93	Graphene oxide assisted spontaneous growth of V ₂ O ₅ nanowires at room temperature. Nanoscale, 2014, 6, 11066-11071.	5.6	27
94	Birch-Type Hydrogenation of Few-Layer Graphenes: Products and Mechanistic Implications. Journal of the American Chemical Society, 2016, 138, 14980-14986.	13.7	27
95	High surface area carbon from polyacrylonitrile for high-performance electrochemical capacitive energy storage. Journal of Materials Chemistry A, 2016, 4, 18294-18299.	10.3	27
96	Molecular beam epitaxy of large-area SnSe ₂ with monolayer thickness fluctuation. 2D Materials, 2017, 4, 014006.	4.4	27
97	Self-Assembled Monolayers on Pt(111):Â Molecular Packing Structure and Strain Effects Observed by Scanning Tunneling Microscopy. Journal of the American Chemical Society, 2006, 128, 5745-5750.	13.7	26
98	Polytypism in few-layer gallium selenide. Nanoscale, 2020, 12, 8563-8573.	5.6	26
99	Synthesis of two-dimensional MoS2/graphene heterostructure by atomic layer deposition using MoF6 precursor. Applied Surface Science, 2019, 494, 591-599.	6.1	25
100	van der Waals Epitaxial Formation of Atomic Layered α-MoO ₃ on MoS ₂ by Oxidation. ACS Applied Materials & Interfaces, 2020, 12, 22029-22036.	8.0	25
101	Synthesis and Properties of Two Dimensional Doped Transition Metal Dichalcogenides. Applied Microscopy, 2017, 47, 19-28.	1.4	25
102	Tensile behavior of Al1â `Mo crystalline and amorphous thin films. Acta Materialia, 2013, 61, 1432-1443.	7.9	24
103	Orientation-dependent optical characterization of atomically thin transition metal ditellurides. Nanoscale, 2018, 10, 21978-21984.	5.6	24
104	Nanocrystalline–amorphous transitions in Al–Mo thin films: Bulk and surface evolution. Acta Materialia, 2009, 57, 4296-4303.	7.9	23
105	Transient SHG Imaging on Ultrafast Carrier Dynamics of MoS ₂ Nanosheets. Advanced Materials, 2018, 30, e1705190.	21.0	23
106	Active Pixel Sensors for electron microscopy. Nuclear Instruments and Methods in Physics Research, Section A: Accelerators, Spectrometers, Detectors and Associated Equipment, 2007, 579, 891-894.	1.6	22
107	High-Angle Tilt Boundary Graphene Domain Recrystallized from Mobile Hot-Wire-Assisted Chemical Vapor Deposition System. Nano Letters, 2014, 14, 4352-4359.	9.1	22
108	The Hide-and-Seek of Grain Boundaries from Moiré Pattern Fringe of Two-Dimensional Graphene. Scientific Reports, 2015, 5, 12508.	3.3	21

#	Article	IF	CITATIONS
109	Line-defect mediated formation of hole and Mo clusters in monolayer molybdenum disulfide. 2D Materials, 2016, 3, 014002.	4.4	21
110	Concentric and Spiral Few-Layer Graphene: Growth Driven by Interfacial Nucleation vs Screw Dislocation. Chemistry of Materials, 2018, 30, 6858-6866.	6.7	21
111	Precise Layer Control and Electronic State Modulation of a Transition Metal Dichalcogenide via Phaseâ€Transitionâ€Induced Growth. Advanced Materials, 2022, 34, e2103286.	21.0	21
112	In situ surface cleaning on a Ge substrate using TMA and MgCp ₂ for HfO ₂ -based gate oxides. Journal of Materials Chemistry C, 2015, 3, 4852-4858.	5.5	20
113	Substantial improvements of long-term stability in encapsulation-free WS ₂ using highly interacting graphene substrate. 2D Materials, 2017, 4, 011007.	4.4	20
114	Vertically oriented MoS ₂ /WS ₂ heterostructures on reduced graphene oxide sheets as electrocatalysts for hydrogen evolution reaction. Materials Chemistry Frontiers, 2021, 5, 3396-3403.	5.9	20
115	Increasing reversible capacity of soft carbon anode by phosphoric acid treatment. Electrochimica Acta, 2014, 146, 630-637.	5.2	19
116	Synthesis and ferromagnetism of Co-doped TiO2â^'δ nanobelts by metallorganic chemical vapor deposition. Applied Physics Letters, 2008, 92, 122508.	3.3	18
117	Microstructural Effects on the Creep Deformation of Alumina/Singleâ€Wall Carbon Nanotubes Composites. Journal of the American Ceramic Society, 2010, 93, 2042-2047.	3.8	18
118	Ferroelectric Tunnel Junction for Dense Cross-Point Arrays. ACS Applied Materials & Interfaces, 2015, 7, 22348-22354.	8.0	18
119	Singleâ€Crystalline Nanobelts Composed of Transition Metal Ditellurides. Advanced Materials, 2018, 30, e1707260.	21.0	18
120	Electrically Robust Singleâ€Crystalline WTe ₂ Nanobelts for Nanoscale Electrical Interconnects. Advanced Science, 2019, 6, 1801370.	11.2	17
121	Tailoring the microstructure and surface morphology of metal thin films for nano-electro-mechanical systems applications. Nanotechnology, 2008, 19, 125705.	2.6	16
122	Direct Fabrication of Zero- and One-Dimensional Metal Nanocrystals by Thermally Assisted Electromigration. ACS Nano, 2010, 4, 2999-3004.	14.6	16
123	Double-Spiral Hexagonal Boron Nitride and Shear Strained Coalescence Boundary. Nano Letters, 2019, 19, 4229-4236.	9.1	15
124	Resonance properties and microstructure of ultracompliant metallic nanoelectromechanical systems resonators synthesized from Al–32at.%Mo amorphous-nanocrystalline metallic composites. Applied Physics Letters, 2008, 92, .	3.3	14
125	Direct imaging and chemical analysis of unstained DNA origami performed with a transmission electron microscope. Chemical Communications, 2011, 47, 9375.	4.1	14
126	A high-performance transparent graphene/vertically aligned carbon nanotube (VACNT) hybrid electrode for neural interfacing. RSC Advances, 2017, 7, 3273-3281.	3.6	14

#	Article	IF	CITATIONS
127	Improved interface quality of atomic-layer-deposited ZrO2 metal-insulator-metal capacitors with Ru bottom electrodes. Thin Solid Films, 2020, 701, 137950.	1.8	14
128	Silicene on Other Two-dimensional Materials: Formation of Heterostructure. Applied Microscopy, 2014, 44, 123-132.	1.4	14
129	Synthesis and characterization of Au–Ta nanocomposites for nanomechanical cantilever devices. Nanotechnology, 2007, 18, 355303.	2.6	13
130	Very high frequency plasma reactant for atomic layer deposition. Applied Surface Science, 2016, 387, 109-117.	6.1	13
131	The Origin of Improved Electrical Double‣ayer Capacitance by Inclusion of Topological Defects and Dopants in Graphene for Supercapacitors. Angewandte Chemie, 2016, 128, 14026-14031.	2.0	13
132	Transition Metal-Based Thiometallates as Surface Ligands for Functionalization of All-Inorganic Nanocrystals. Chemistry of Materials, 2017, 29, 10510-10517.	6.7	13
133	Unraveling the Water Impermeability Discrepancy in CVDâ€Grown Graphene. Advanced Materials, 2018, 30, e1800022.	21.0	13
134	Reaction Mechanism of Pt Atomic Layer Deposition on Various Textile Surfaces. Chemistry of Materials, 2019, 31, 8995-9002.	6.7	13
135	Ultrahigh Strength and Modulus Grapheneâ€Based Hybrid Carbons with AB tacked and Turbostratic Structures. Advanced Functional Materials, 2020, 30, 2005381.	14.9	13
136	Defect-gradient-induced Rashba effect in van der Waals PtSe2 layers. Nature Communications, 2022, 13, 2759.	12.8	13
137	Superstructural defects and superlattice domains in stacked graphene. Carbon, 2014, 80, 755-761.	10.3	12
138	Effects of dry oxidation treatments on monolayer graphene. 2D Materials, 2017, 4, 024011.	4.4	12
139	Interfaceâ€Driven Partial Dislocation Formation in 2D Heterostructures. Advanced Materials, 2019, 31, e1807486.	21.0	11
140	Design of 2D Layered Catalyst by Coherent Heteroepitaxial Conversion for Robust Hydrogen Generation. Advanced Functional Materials, 2021, 31, 2005449.	14.9	11
141	Folding and Fracture of Singleâ€Crystal Graphene Grown on a Cu(111) Foil. Advanced Materials, 2022, 34, e2110509.	21.0	11
142	The influence of inelastic scattering on EFTEM images—exemplified at 20kV for graphene and silicon. Ultramicroscopy, 2013, 134, 102-112.	1.9	10
143	Surface treatment process applicable to next generation graphene-based electronics. Carbon, 2016, 104, 119-124.	10.3	10
144	The impact of substrate surface defects on the properties of two-dimensional van der Waals heterostructures. Nanoscale, 2018, 10, 19212-19219.	5.6	10

#	Article	IF	CITATIONS
145	Surface Energy Change of Atomic-Scale Metal Oxide Thin Films by Phase Transformation. ACS Nano, 2020, 14, 676-687.	14.6	10
146	Anisotropic Angstrom-Wide Conductive Channels in Black Phosphorus by Top-down Cu Intercalation. Nano Letters, 2021, 21, 6336-6342.	9.1	10
147	Spiral Growth of Adlayer Graphene. Advanced Materials, 2022, 34, e2107587.	21.0	10
148	The influence of Sc on thermal stability of a nanocrystalline Al-Mg alloy processed by cryogenic ball milling. Metallurgical and Materials Transactions A: Physical Metallurgy and Materials Science, 2005, 36, 1587-1594.	2.2	9
149	Enhanced Photocatalytic Properties of TiO2Nanobelts via In Situ Doping of C and Fe. Journal of the Electrochemical Society, 2011, 159, K42-K45.	2.9	9
150	Spontaneous Formation of a ZnO Monolayer by the Redox Reaction of Zn on Graphene Oxide. ACS Applied Materials & Interfaces, 2020, 12, 54222-54229.	8.0	9
151	Synthesis of Highly Oriented Graphite Films with a Low Wrinkle Density and Near-Millimeter-Scale Lateral Grains. Chemistry of Materials, 2020, 32, 3134-3143.	6.7	9
152	Phase Transformation of Two-Dimensional Transition Metal Dichalcogenides. Applied Microscopy, 2018, 48, 43-48.	1.4	9
153	Co clustering and ferromagnetism in chemical vapor deposited Ti1â^xCoxO2â^î^ thin films. Applied Physics Letters, 2007, 90, 102504.	3.3	8
154	Nanoindentation properties and the microstructure of grain boundary precipitate-free zones (PFZs) in an AlCuSiGe alloy. Philosophical Magazine, 2007, 87, 3905-3919.	1.6	8
155	Effects of surface ligands on the charge memory characteristics of CdSe/ZnS nanocrystals in TiO2 thin film. Applied Physics Letters, 2009, 95, 183111.	3.3	8
156	An Improved Specimen Preparation of Porous Powder Materials for Transmission Electron Microscopy. Microscopy and Microanalysis, 2014, 20, 366-367.	0.4	8
157	A Facile Route for Patterned Growth of Metal–Insulator Carbon Lateral Junction through One-Pot Synthesis. ACS Nano, 2015, 9, 8352-8360.	14.6	8
158	Atomic Resolution Imaging of Rotated Bilayer Graphene Sheets Using a Low kV Aberration-corrected Transmission Electron Microscope. Applied Microscopy, 2012, 42, 218-222.	1.4	8
159	Growth and Selective Etching of Twinned Graphene on Liquid Copper Surface. Small, 2021, 17, 2103484.	10.0	7
160	Effective Passivation of Black Phosphorus under Ambient Conditions. Applied Microscopy, 2017, 47, 176-186.	1.4	7
161	Atomic-scale characterization of plasma-induced damage in plasma-enhanced atomic layer deposition. Applied Surface Science, 2017, 425, 781-787.	6.1	6
162	In Situ Scanning Transmission Electron Microscopy Study of MoS ₂ Formation on Graphene with a Deep-Learning Framework. ACS Omega, 2021, 6, 21623-21630.	3.5	6

#	Article	IF	CITATIONS
163	Electrochemical Formation of a Covalent–Ionic Stage-1 Graphite Intercalation Compound with Trifluoroacetic Acid. Chemistry of Materials, 2022, 34, 217-231.	6.7	6
164	Atomic structural variations of [0001]-tilt grain boundaries during ZnO grain growth occurred by thermal treatments. Applied Surface Science, 2011, 257, 4817-4820.	6.1	5
165	Thiometallate precursors for the synthesis of supported Pt and PtNi nanoparticle electrocatalysts: Size-focusing by S capping. Nanoscale, 2020, 12, 10498-10504.	5.6	5
166	Atomic Arrangements of Graphene-like ZnO. Nanomaterials, 2021, 11, 1833.	4.1	5
167	Quantitative Evaluation of Dislocation Density in Epitaxial GaAs Layer on Si Using Transmission Electron Microscopy. Applied Microscopy, 2014, 44, 74-78.	1.4	5
168	A Study on the H3PO4-Treated Soft Carbon as Anode Materials for Lithium Ion Batteries. Journal of the Korean Electrochemical Society, 2012, 15, 207-215.	0.1	5
169	In situ tensile and fracture behavior of monolithic ultra-thin amorphous carbon in TEM. Carbon, 2022, 196, 236-242.	10.3	5
170	Experiment and FEM Analysis of Tensile Behavior of Bimodal Nanocrystalline Al-Mg Alloys. Materials Research Society Symposia Proceedings, 2004, 821, 30.	0.1	4
171	Epitaxial Growth of ZnO Monolayer on Graphene: The Thinnest Metal Oxide Semiconductor. Microscopy and Microanalysis, 2017, 23, 1434-1435.	0.4	4
172	Investigation of the Microstructure of Laser-Arc Hybrid Welded Boron Steel. Jom, 2018, 70, 1548-1553.	1.9	4
173	Dedicated preparation for in situ transmission electron microscope tensile testing of exfoliated graphene. Applied Microscopy, 2019, 49, 3.	1.4	4
174	Synthesis of high-quality monolayer graphene by low-power plasma. Current Applied Physics, 2019, 19, 44-49.	2.4	4
175	Novel high-k gate dielectric properties of ultrathin hydrocarbon films for next-generation metal-insulator-semiconductor devices. Carbon, 2020, 158, 513-518.	10.3	4
176	Contrast Transfer Function-Based Exit-Wave Reconstruction and Denoising of Atomic-Resolution Transmission Electron Microscopy Images of Graphene and Cu Single Atom Substitutions by Deep Learning Framework. Nanomaterials, 2020, 10, 1977.	4.1	4
177	Bimodal Microstructures in Nanocrystalline Al and Al-Mg Alloy Powders Prepared by Cryogenic Ball Milling. Materials Research Society Symposia Proceedings, 2004, 821, 185.	0.1	3
178	Thermomagnetic Analysis of Nanocrystalline Nd _{4.5} Fe ₇₇ B _{18.5} Alloy. Materials Transactions, 2009, 50, 2302-2307.	1.2	3
179	Atomic Resolution Imaging and Spectroscopy of Graphene Using the TEAM 0.5. Microscopy and Microanalysis, 2009, 15, 124-125.	0.4	3
180	Nanographitic layer-mediated synthesis of carbon-TiO2 hybrid nanobelts by metalorganic chemical vapor deposition. Materials Letters, 2012, 81, 20-22.	2.6	3

#	Article	IF	CITATIONS
181	Mapping Graphene Grain Orientation by the Growth of WS ₂ Films with Oriented Cracks. Chemistry of Materials, 2020, 32, 7484-7491.	6.7	3
182	Antiphase Boundaries as Faceted Metallic Wires in 2D Transition Metal Dichalcogenides. Advanced Science, 2020, 7, 2000788.	11.2	3
183	Study of Nd-Fe-B alloys with nonstoichiometric Nd content in optimal magnetic state. Science of Sintering, 2009, 41, 209-218.	1.4	3
184	Unconventional assemblies of bisacylhydrazones: The role of water for circularly polarized luminescence. Aggregate, 2022, 3, .	9.9	3
185	Observation of the Initial Stage of 3C-SiC Heteroepitaxial Growth on the Si Nanomembrane. Crystal Growth and Design, 2022, 22, 1421-1426.	3.0	3
186	Bimodal Structured Bulk Nanocrystalline Al-7.5Mg Alloy. Materials Research Society Symposia Proceedings, 2003, 791, 1.	0.1	2
187	Observation of spin-polarized Anderson state around charge neutral point in graphene with Fe-clusters. Scientific Reports, 2020, 10, 4784.	3.3	2
188	Epitaxially grown copper phosphide (Cu3P) nanosheets nanoarchitecture compared with film morphology for energy applications. Surfaces and Interfaces, 2021, 26, 101369.	3.0	2
189	Bimodal Microstructure and Mechanical Properties of Cryomilled Nanocrystalline Al-7.5Mg. Materials Research Society Symposia Proceedings, 2002, 740, 1.	0.1	1
190	Development of a radiation hard CMOS monolithic pixel sensor. , 2008, , .		1
191	Graphene: Unraveling the Water Impermeability Discrepancy in CVD-Grown Graphene (Adv. Mater.) Tj ETQq1 1 (0.784314 21.0	rgBT /Overloc
192	Direct observation of leakage currents in a metal–insulator–metal capacitor using <i>in situ</i> transmission electron microscopy. Nanotechnology, 2018, 29, 435705.	2.6	1
193	A novel specimen preparation of porous cathode materials in lithium-ion batteries for high-resolution transmission electron microscopy. Materials Characterization, 2019, 155, 109804.	4.4	1
194	Metallic Transitionâ€Metal Chalcogenides: Electrically Robust Singleâ€Crystalline WTe ₂ Nanobelts for Nanoscale Electrical Interconnects (Adv. Sci. 3/2019). Advanced Science, 2019, 6, 1970017.	11.2	1
195	Selfâ€Powered Gas Sensors: 2D Transition Metal Dichalcogenide Heterostructures for p―and nâ€Type Photovoltaic Selfâ€Powered Gas Sensor (Adv. Funct. Mater. 43/2020). Advanced Functional Materials, 2020, 30, 2070284.	14.9	1
196	Investigation of Oxide Phases of MoS2: van der Waals Epitaxially Formed α-MoO3 on MoS2. Microscopy and Microanalysis, 2021, 27, 646-647.	0.4	1
197	Formation Dynamics of Carbon Atomic Chain from Graphene by Electron Beam Irradiation. Applied Microscopy, 2018, 48, 126-127.	1.4	1
198	Elucidation of Novel Potassium-Mediated Oxidation and Etching of Two-Dimensional Transition Metal Dichalcogenides. ACS Applied Materials & Interfaces, 2021, 13, 49163-49171.	8.0	1

#	Article	IF	CITATIONS
199	Silica Particleâ€Mediated Growth of Single Crystal Graphene Ribbons on Cu(111) Foil. Small, 2022, , 2202536.	10.0	1
200	In-Situ TEM Observation of Metal Zn Nanocrystal Growth on ZnO Films. Microscopy and Microanalysis, 2009, 15, 698-699.	0.4	0
201	Direct Mapping of Stacking Structure in Rotated Bilayer Graphene Using Aberration-corrected Transmission Electron Microscopy. Microscopy and Microanalysis, 2013, 19, 1226-1227.	0.4	0
202	B21-O-03The Identification of Grain Boundaries in Two-dimensional Graphene using Moire Pattern Fringe. Microscopy (Oxford, England), 2015, 64, i40.2-i40.	1.5	0
203	Microstructural Investigation on Degradation Mechanism of Layered LiNi 0.6 Co 0.2 Mn 0.2 O 2 Cathode Materials by Analytical TEM/STEM. Microscopy and Microanalysis, 2016, 22, 1336-1337.	0.4	0
204	Carrier Dynamics: Transient SHG Imaging on Ultrafast Carrier Dynamics of MoS2 Nanosheets (Adv.) Tj ETQq0 0 0	rgBT/Ove 21.0	erlock 10 Tf S
205	Local Lattice Match for Commensurate State of Graphene/h-BN van der Waals Heterostructure with TEM Analysis. Microscopy and Microanalysis, 2018, 24, 1616-1617.	0.4	0
206	Monolayer-like Behavior of Bilayer Transition-Metal Dichalcogenides. Microscopy and Microanalysis, 2019, 25, 1780-1781.	0.4	0
207	The Third Eastâ€Asia Microscopy Conference (EAMC3). Microscopy Research and Technique, 2019, 82, 3-3.	2.2	0
208	Formation of two-dimensional MoS2 and one-dimensional MoO2 nanowire hybrids. Applied Microscopy, 2019, 49, 16.	1.4	0
209	Grapheneâ€Based Hybrid Carbons: Ultrahigh Strength and Modulus Grapheneâ€Based Hybrid Carbons with ABâ€Stacked and Turbostratic Structures (Adv. Funct. Mater. 50/2020). Advanced Functional Materials, 2020, 30, 2070334.	14.9	0
210	Growth and Selective Etching of Twinned Graphene on Liquid Copper Surface (Small 40/2021). Small, 2021, 17, .	10.0	0
211	The First Transmission Electron Microscope Image Imagined by Artificial Intelligence. Applied Microscopy, 2017, 47, 251-252.	1.4	0

OH molecule-involved formation of point defects in monolayer graphene. Nanotechnology, 2021, 32, 025704. 2.6 0